

pubs.acs.org/JACS Article

# Anhydrous Proton Transport within Phosphonic Acid Layers in Monodisperse Telechelic Polyethylenes

Anne Staiger, § Benjamin A. Paren, § Robin Zunker, Son Hoang, Manuel Häußler, Karen I. Winey, \* and Stefan Mecking\*



Cite This: J. Am. Chem. Soc. 2021, 143, 16725-16733



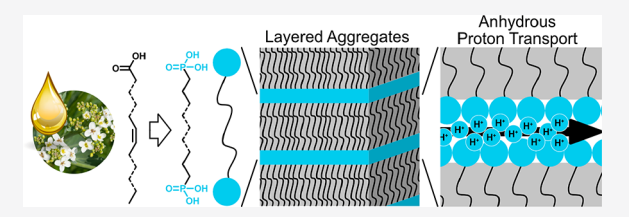
**ACCESS** 

Metrics & More



SI Supporting Information

**ABSTRACT:** Polymers bearing phosphonic acid groups have been proposed as anhydrous proton-conducting membranes at elevated operating temperatures for applications in fuel cells. However, the synthesis of phosphonated polymers and the control over the nanostructure of such polymers is challenging. Here, we report the straightforward synthesis of phosphonic acid-terminated, long-chain aliphatic materials with precisely 26 and 48 carbon atoms ( $C_{26}PA_2$  and  $C_{48}PA_2$ ). These materials combine the structuring ability of mono-



disperse polyethylenes with the ability of phosphonic acid groups to form strong hydrogen-bonding networks. Anhydride formation is absent so that charge carrier loss by a condensation reaction is avoided even at elevated temperatures. Below the melting temperature  $(T_{\rm m})$ , both materials exhibit a crystalline polyethylene backbone and a layered morphology with planar phosphonic acid aggregates separated by 29 and 55 Å for  $C_{26}PA_2$  and  $C_{48}PA_2$ , respectively. Above  $T_{\rm m}$ , the amorphous polyethylene (PE) segments coexist with the layered aggregates. This phenomenon is especially pronounced for the  $C_{26}PA_2$  and is identified as a thermotropic smectic liquid crystalline phase. Under these conditions, an extraordinarily high correlation length (940 Å) along the layer normal is observed, demonstrating the strength of the hydrogen bond network formed by the phosphonic acid groups. The proton conductivity in both materials in the absence of water reaches  $10^{-4}$  S/cm at 150 °C. These new precise phosphonic acid—based materials illustrate the importance of controlling the chemistry to form self-assembled nanoscale aggregates that facilitate rapid proton conductivity.

## ■ INTRODUCTION

The storage and on-site production of green energy is a major challenge facing the future of energy infrastructure. Fuel cells are among the most promising candidates to meet this increasing demand for energy supply. Much effort is being invested into the search for better proton exchange membranes (PEMs) for the use in fuel cells. State-of-the-art PEMs consist of single-ion conducting polymers (ionomers), which typically have perfluorinated backbones and sulfonic acid groups covalently attached to the polymer backbone, with one of the industry standards being Nafion ®.1-3 Rapid proton transport in ionomers with sulfonic acid groups is enhanced by the presence of water, which leads to the formation of charge carriers in nanoscale hydrophilic domains.4 However, the dependence of proton transport on water restricts the use of such polymer membranes to temperatures below 100 °C at atmospheric pressure. Higher operating temperatures are desirable for many reasons, for example, to prevent catalyst poisoning by the adsorption of fuel impurities or regarding the simultaneous generation of electric and thermal energy. 5,6 Thus, polymers with a high thermal stability and a high proton conductivity in the absence of water are desirable. Recent studies have demonstrated the potential of phosphoric aciddoped polybenzimidazoles as high temperature anhydrous

PEMs, though while proton conductivity is high, these PEMs are vulnerable to acid leaching.  $^{6-8}$ 

To overcome this challenge, polymers bearing covalently bound phosphonic acid groups are promising candidates, as they are resistant to acid leaching, exhibit higher thermal and chemical stability than their sulfonated analogues, and transport protons effectively under both humid and dry conditions. The lower acidity of phosphonic acid compared to sulfonic acid typically leads to lower overall conductivities in phosphonated polymers. However, the self-dissociable, amphoteric nature of phosphonic acid gives rise to well-connected hydrogen-bonded networks in phosphonated polymers and these aggregated phosphonic acid groups are essential for achieving high proton conductivities. A sophisticated design of phosphonated polymers with a high degree of functionalization may capitalize on this hydrogen-bonded network formation and lead to enhanced proton

Received: August 2, 2021 Published: September 29, 2021





Scheme 1. Synthesis of Telechelic Phosphonic Acids Starting from the Respective Telechelic Diol

transport. A complementary approach to accessing highly proton-conducting PEMs is to utilize polymers with ionic functional groups precisely spaced and covalently attached to the polymer backbone.<sup>15</sup> Designing precisely spaced polymers can lead to control over both the ionic aggregate nanostructure and the polymer crystallinity. 16-22 Trigg et al. reported a polyethylene-like material with precisely placed sulfonic acid groups along the backbone, which exhibits a nanoscale layered morphology when hydrated, that results in excellent proton conductivity.<sup>23</sup> However, introduction of phosphonic acid groups to the polymer backbone in a precise way is hampered by several synthetic difficulties, such as the high tendency of the phosphonic acid groups to aggregate and, in the case of polymerization with esterified phosphonic acid derivatives, the harsh conditions necessary to cleave the ester bonds in the polymer. 24-26 These issues and the tedious multistep procedures required have hindered studies of precisely phosphonated polymers synthesized via acyclic diene metathesis (ADMET).27-29

Ionic polymers can form thermotropic liquid crystalline (LC) phases in a temperature range above the crystalline solid and below the isotropic liquid.<sup>30</sup> The intermolecular interactions of the ionic groups and the polymer backbones can lead to the formation of LC nanostructures formed by nanosegregation of the polar and unpolar segments.<sup>31</sup> In proton conductors, the formation of hydrogen-bonded networks by self-induced ordering of the functional groups is favorable with regard to long-range and fast proton transport.<sup>32</sup> Liang et al. reported on phosphonic acid end-functionalized compounds that exhibit thermotropic LC phases at elevated temperatures, forming bilayered assemblies.<sup>33</sup> The beneficial impact of the liquid crystalline phases on the anhydrous proton conductivity was clearly demonstrated.

Polyethylene (PE) based materials are attractive as PEMs due to their ability to crystallize and self-assemble into ordered aggregate morphologies as well as their chemical stability.<sup>34–37</sup> These features can be combined with covalently attached ionic groups in PE telechelics, which contain functional groups as end groups. Telechelic polyethylenes generated by ethylene insertion chain growth have a distribution of chain lengths, even from living catalytic chain transfer protocols.<sup>38–40</sup> We recently reported an alternative route to polyethylene telechelics, giving access to end group functionalized and low molecular weight PE with precise chain lengths, e.g., 48 carbon atoms. This scalable approach is based on entirely catalytic reactions starting from common plant based fatty acids as a feedstock. 17,41,42 The precisely monodisperse backbones crystallize in a polyethylene-like orthorhombic motif, resulting in layers of functional groups alternating with highly crystalline extended-chain polymer segments as demonstrated for

carboxylate- and sulfonate-terminated telechelics with alkaline metal counterions. <sup>17,41</sup> For these monovalent end groups, the hydrocarbon segments are still able to exhibit order even though the end groups may reduce ordering. For bivalent end groups such as phosphonates, the interplay of charge vs order has yet to be investigated.

We now report monodisperse polyethylene chains with two phosphonic acid end groups that form extended-chain layered aggregates that facilitate the anhydrous transport of protons. These polymers achieve maximum conductivity in the thermotropic liquid crystalline phase at favorable temperatures around 140  $^{\circ}\mathrm{C}.$ 

# ■ RESULTS AND DISCUSSION

Syntheses of Precise Phosphonic Acid-Terminated Telechelics. The saturated  $C_{26}$  and  $C_{48}$  telechelic starting materials were obtained by reported procedures.<sup>42</sup> Starting from erucic acid, a self-metathesis reaction directly yields the  $\rm C_{26}$  building block precursor. A further dynamic catalytic crystallizing double bond isomerization step followed by an effective olefin self-metathesis resulted in "chain doubling" to the C48 precursor. Subsequent hydrogenation of the double bond and reduction of the acid ester end groups yields the respective  $C_{26}$  and  $C_{48}$  diols,  $C_{26}(OH)_2$  and  $C_{48}(OH)_2$ . Reaction conditions were established for increased batch sizes and the workup was simplified compared to the original procedure (see Supporting Information for details). Note that this synthetic approach is transferable to other fatty acid substrates, giving access to multiple chain lengths of the polyethylene. The end group modification of the polyethylenelike telechelics is challenging due to their limited solubility and the difficulty to separate starting materials from the products in case of non-quantitative conversions. Therefore, reaction conditions were implemented for all reaction steps that meet the following demands: sufficient solubility of the starting materials, quantitative conversions, simple workup conditions and applicability to increased batch sizes. The conversion to  $C_{26}Br_2$  and  $C_{48}Br_2$ , which was originally performed by an Appel reaction of C<sub>48</sub>(OH)<sub>2</sub> with CBr<sub>4</sub> and PPh<sub>3</sub>,<sup>41</sup> was replaced by a more atom-efficient bromination with phosphorus tribromide in toluene (Scheme 1). The purification of the product included the hot filtration over a short plug of silica and recrystallization from the solution. This yielded the pure C<sub>26</sub>Br<sub>2</sub> and C<sub>48</sub>Br<sub>2</sub>. The conversion of the end groups was monitored by <sup>1</sup>H nuclear magnetic resonance (NMR) spectroscopy via the indicative high-field shift of the  $\alpha$ methylene resonance from 3.7 to 3.4 ppm (in tetrachloroethane-d<sub>2</sub> at 110 °C). Phosphonate ester groups were introduced by a Michaelis-Arbuzov reaction with triethyl phosphite to quantitatively yield  $C_{26}(PO(OEt)_2)_2$  and

 $C_{48}(PO(OEt)_2)_2$ . Excessive triethyl phosphite was distilled off after the reaction was completed. The end groups' <sup>31</sup>P NMR resonance (31.4 and 30.8 ppm for  $C_{26}(PO(OEt)_2)_2$  and  $C_{48}(PO(OEt)_2)_2$ , respectively, in dmso- $d_6$  at 110 °C agrees with reported values for other alkyl diethylphosphonates (typically measured in chloroform- $d_1$ , 32.4 ppm). <sup>44</sup> The crude materials were used in the following McKenna deprotection without further purification. The desired  $C_{26}(PO(OH)_2)_2$  and  $C_{48}(PO(OH)_2)_2$  (abbreviated as  $C_{26}PA_2$  and  $C_{48}PA_2$ ) were obtained by phosphonate ester cleavage by McKenna reactions with trimethylsilyl bromide under mild conditions and subsequent protonation in a water/methanol mixture. <sup>45</sup> The hydrolysis reaction was monitored by <sup>31</sup>P NMR at 110 °C in dmso- $d_6$ . <sup>31</sup>P NMR shifts of the products agree with an n-tetradecylphosphonic acid reference (Figure 1, see

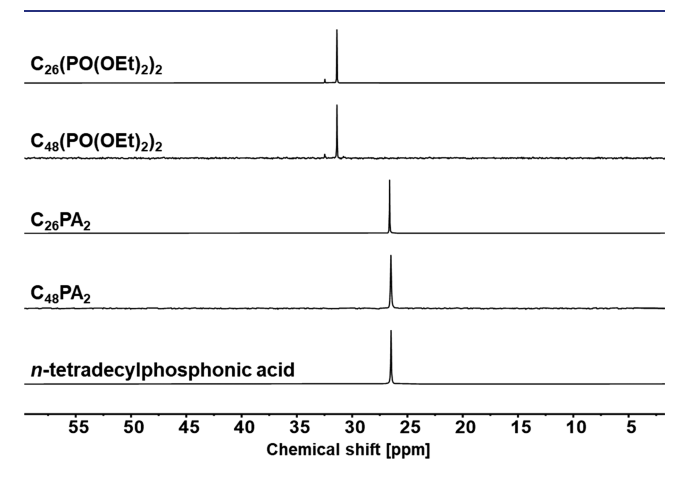


**Figure 1.**  $^{31}$ P NMR at 110  $^{\circ}$ C in dmso- $d_{6}$  of the synthesized telechelic phosphonate esters and telechelic phosphonic acids. As a reference, *n*-tetradecylphosphonic acid is shown.

Figures S21 to S26 in the Supporting Information for full NMR characterization of  $C_{26}PA_2$  and  $C_{48}PA_2$ ). In further purification by recrystallization from methanol, the limited solubility of the products was overcome by working at temperatures above the solvent boiling point in a microwave reactor with an operating pressure of up to 30 bar. This yielded the target products in high purity. No additional, high field shifted  $^{31}P$  NMR signals were detected, unlike reported for poly(vinylphosphonic acid).  $^{46}$  Therefore, a formation of

anhydrides by condensation of the phosphonic acid groups during the synthesis and purification steps can be excluded.

**Thermal Analysis.** Thermogravimetric analysis (TGA) under a nitrogen atmosphere and air provided insights on the thermal stability of the telechelic phosphonic acid materials C<sub>26</sub>PA<sub>2</sub> and C<sub>48</sub>PA<sub>2</sub> (Figure 2). For both materials, only trace weight loss is observed up to 200 °C, which may be due to traces of residual solvent. The telechelics do not undergo significant condensation reactions below 200 °C. Decomposition under a nitrogen atmosphere occurs at onset temperatures of 467 and 454 °C (C<sub>26</sub>PA<sub>2</sub> and C<sub>48</sub>PA<sub>2</sub>, respectively) with low residual mass, presumably originating from non-volatile inorganic phosphorus oxides. The decomposition under air exhibits comparable onset temperatures to those under a nitrogen, and was previously reported for 1heptylphosphonic acid to be a result of the polyethylene chain oxidation.<sup>47</sup> Between 200 and 450 °C, a material weight loss of approximately 5% is observed for both C<sub>26</sub>PA<sub>2</sub> and C<sub>48</sub>PA<sub>2</sub>. Complete condensation reaction of the phosphonic acid functional groups would account for a material weight loss of 6.8% and 4.3% (C<sub>26</sub>PA<sub>2</sub> and C<sub>48</sub>PA<sub>2</sub>, respectively). The observed weight loss in this temperature region being in this range suggests it likely arises from condensation reactions. A final decomposition step is observed under both nitrogen (~880 °C) and air (~580 °C). The thermal stability of the materials toward the formation of anhydrides was further investigated by <sup>31</sup>P NMR spectroscopy. Both phosphonic acid materials were held in closed vials for 4, 24, 72, and 96 h at 140 °C and subsequently dissolved in dmso-d<sub>6</sub> for NMR analysis at 110 °C. A high-field shifted additional phosphorus resonance would be expected for the phosphonic acid anhydride formed by condensation reactions. 46 Both C<sub>26</sub>PA<sub>2</sub> and C<sub>48</sub>PA<sub>2</sub> feature only the unaltered sharp resonance of the starting material at 26.6 ppm (C<sub>26</sub>PA<sub>2</sub>) and 27.2 ppm (C<sub>48</sub>PA<sub>2</sub>) (see Figure S1), confirming that the phosphonic acid functionalized polyethylene chains do not undergo condensation reactions below 200 °C.

The phase transitions of  $C_{26}PA_2$  and  $C_{48}PA_2$ , respectively, as observed in DSC thermograms differ significantly (Figure 3 and summarized in Table 1). Distinct and reversible transitions are observed between 110 and 160 °C for both  $C_{26}PA_2$  and  $C_{48}PA_2$ , associated with changes in the polyethylene backbones, as corroborated by X-ray scattering results presented below.  $C_{26}PA_2$  exhibits a double melting peak  $(T_m)$  at 150.0–

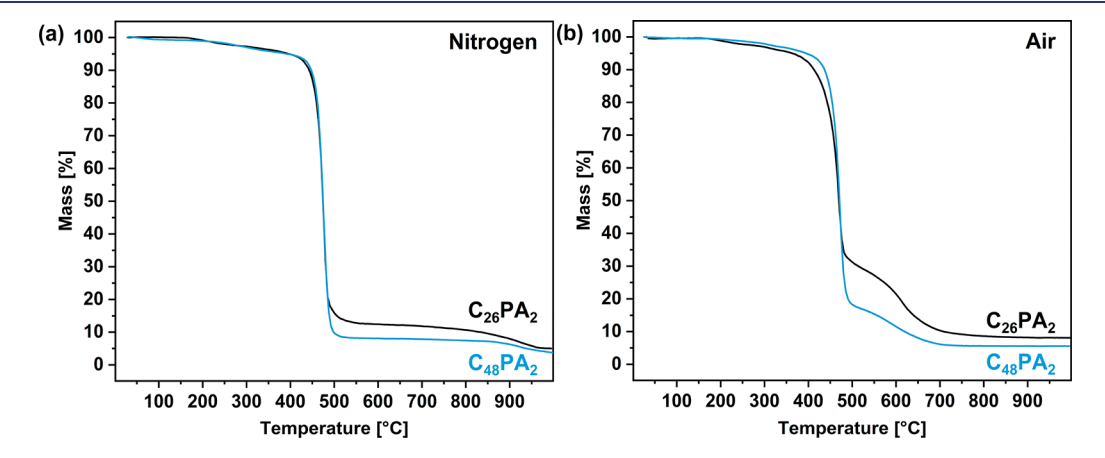
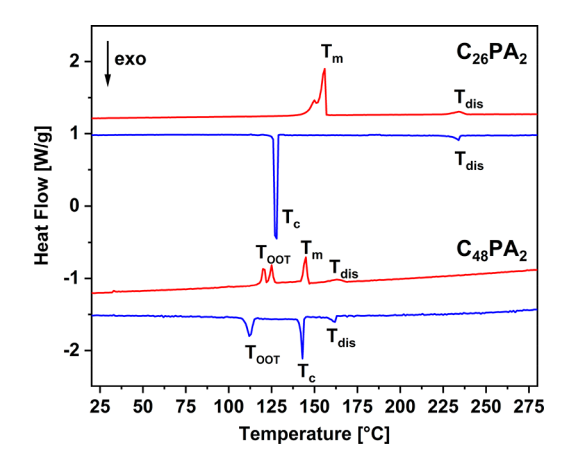


Figure 2. TGA thermal graphs of  $C_{26}PA_2$  (black) and  $C_{48}PA_2$  (blue) at a heating rate of 10 °C/min from 30 to 1000 °C under a constant stream of (a) nitrogen and (b) air.



**Figure 3.** DSC traces of  $C_{26}PA_2$  (top) and  $C_{48}PA_2$  (bottom) from 0 to 280 °C (second heating/cooling cycle, heating/cooling rate of 1 °C/min). Red curves represent heating, blue curves represent cooling process. Data were shifted vertically for clarity.

Table 1. Thermal Properties of the Monodisperse Telechelic Polyethylenes with Phosphonic acids<sup>a</sup>

	C <sub>26</sub> PA <sub>2</sub>		$C_{48}PA_2$	
	Heating	Cooling	Heating	Cooling
$T_{\text{OOT}}$ (°C)			120.5, 124.9	112.0
$T_{\mathrm{m}}$ or $T_{\mathrm{c}}$ (°C)	150.0, 155.7	127.6	145.0	142.8
$T_{\rm dis}$ (°C)	234.1	234.0	163.0	161.5

 $^a$ The transition temperatures reported are from the 2nd heating and 2nd cooling cycles in DSC.

155.7 °C, and a crystallization temperature  $(T_c)$  at 127.6 °C.  $C_{48}PA_2$  has a similar  $T_m$  at 145 °C, but the  $T_c$  (143 °C) is nearly the same as the melting point. We attribute both the higher  $T_m$  and lower  $T_c$  in  $C_{26}PA_2$  to the higher concentration of phosphonic acid groups, which will impede the melting and crystallization processes of the polyethylene backbone. Much higher melting points between 200 and 220 °C have been reported for the small molecules C<sub>4</sub>PA<sub>2</sub> to C<sub>12</sub>PA<sub>2</sub>, likely due to the even higher concentration of phosphonic acid groups, whose aggregates similarly impede the melting process. There are also order-to-order transitions  $(T_{OOT})$  in  $C_{48}PA_2$ below the melting point, which result from transitions between crystal structures in the polyethylene backbone. Though we are able to identify the peaks corresponding to melting and crystallization of the polyethylene backbone, the melting enthalpy is challenging to assign due to overlapping transitions, as well as intermediate transitions between crystal structures.

For both materials, an additional endothermic process is visible at temperatures above the melting temperatures of the PE backbones,  $T_{\rm dis}$  (234 and 162 °C for  $C_{26}PA_2$  and  $C_{48}PA_2$  during cooling, respectively). At these temperatures, the hydrogen bond network formed by the phosphonic acid groups transitions into a disordered state and occurs at the same temperature on heating and cooling. This behavior was studied in detail by X-ray scattering and by polarized light microscopy, as discussed below.

**Morphology.** The hierarchical morphologies of the two precise telechelic phosphonate polyethylenes are a result of the interplay between the van-der-Waals forces between the nonpolar polyethylene segments and the polar interactions of the phosphonic acid groups. By combining temperature dependent X-ray scattering studies with polarized light microscopy (PLM)

we gained insight into the nanoscale structures and morphological transitions present in these materials. Figure 4

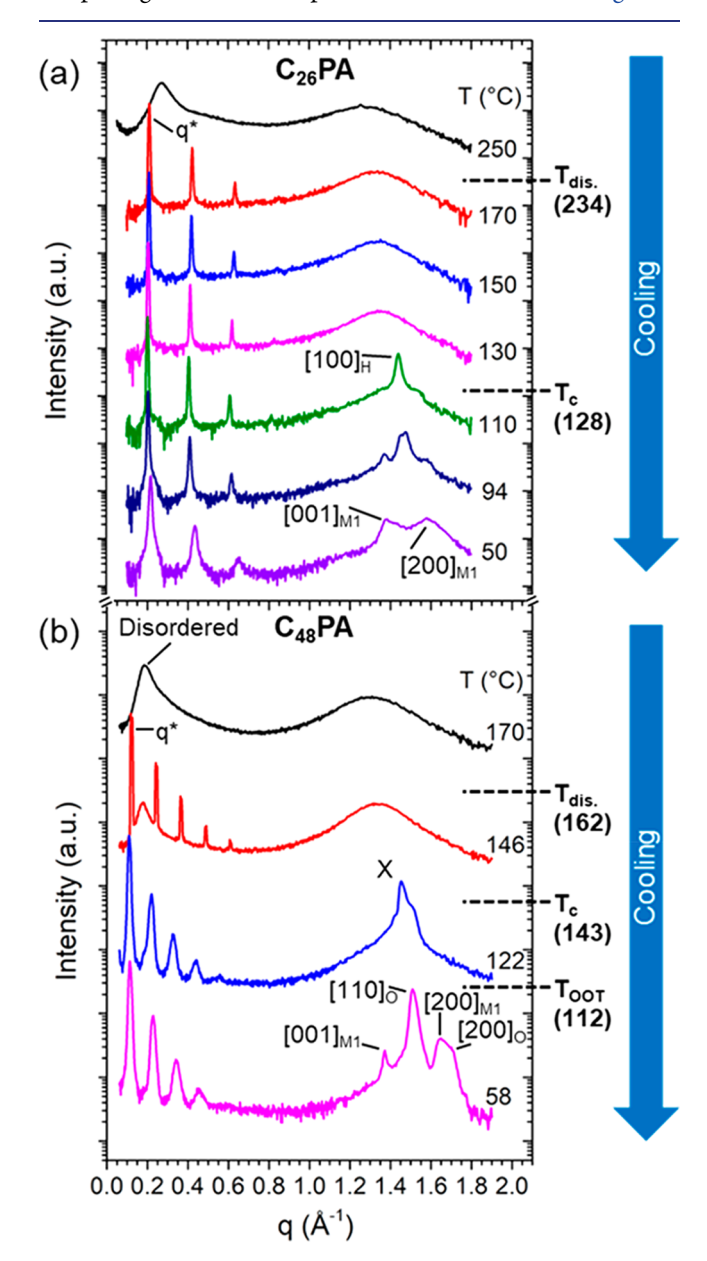


**Figure 4.** X-ray scattering profiles of (a)  $C_{26}PA_2$  and (b)  $C_{48}PA_2$  at selected temperatures upon cooling. Reflections at q>1.0 Å $^{-1}$  indicate chain packing as Hex, M1, O and X, representing hexagonal, monoclinic, orthorhombic and an unknown phase, respectively. Data was shifted vertically for clarity. Transition temperatures from DSC measurements (on cooling) are noted.

shows the X-ray scattering profiles of  $C_{26}PA_2$  and  $C_{48}PA_2$  at selected temperatures during cooling from above  $T_{\rm dis}$ . At high temperatures, both  $C_{26}PA_2$  and  $C_{48}PA_2$  exhibit only a broad amorphous halo centered at  $q \sim 1.3~{\rm \AA}^{-1}$ , indicating melted polyethylene segments. Additionally, both polymers exhibit a broad, asymmetric peak at  $q \sim 0.2-0.3~{\rm \AA}^{-1}$ , which corresponds to the disordered packing of the phosphonic acid groups. Upon cooling, transitions in the polymers are consistent with the DSC results. We also note that the morphologies in both polymers are fully reversible with some hysteresis in  $C_{26}PA_2$  upon heating to 170 °C (Figure S4) and

this is discussed with regard to proton conductivity in the following section.

When the polyethylene backbone is still in the melt state in both  $C_{26}PA_2$  and  $C_{48}PA_2$ , sharp equidistant peaks appear upon cooling below  $T_{\rm dis}$ , in the low q-range with ratios of 1:2:3:4:5, relative to q\*, which indicates the presence of layered aggregate morphologies. This derives from a nanophase separation of the acidic end-groups from the PE chains into layered aggregates as reported before for phosphonated polymers and for the carboxylic acid analogues  $C_{21}(\text{COOH})_2$  and  $C_{46}(\text{COOH})_2$ . Upon further cooling, the layered aggregate morphologies persist as the polymers crystallize and experience additional order-to-order transitions.

The alkyl chain packing behavior of C<sub>26</sub>PA<sub>2</sub> becomes semicrystalline with a hexagonal crystal structure upon cooling below 130 °C, followed by an order-to-order transition to a monoclinic phase crystal structure at lower temperatures. This hexagonal to monoclinic transition does not appear in the DSC trace, which may be because the transition is occurring over a wide range of temperatures. In the case of C<sub>48</sub>PA<sub>2</sub>, an unidentified semicrystalline structure (indicated as X on Figure 4) forms first upon cooling from the melt state and the PE chains transition into coexisting monoclinic and orthorhombic phases (detailed positions of all observed reflections at the selected temperatures can be found in the Supporting Information, Table S1 and Table S2). The previously reported carboxylic acid analogues  $C_{21}(COOH)_2$  and  $C_{46}(COOH)_2$ both show an orthorhombic PE crystallinity at all temperatures below the melting transition, while a monoclinic structure of the PE backbones was also observed in the zinc carboxylate analogue, C<sub>46</sub>(COO)<sub>2</sub>Zn.<sup>17</sup> The larger bivalent functional groups require a larger headgroup separation that induces monoclinic packing of the PE chains. 48 Similarly, relative to the carboxylic acid groups the large phosphonic acid groups in C<sub>26</sub>PA<sub>2</sub> and C<sub>48</sub>PA<sub>2</sub> produce monoclinic crystals.

The center-to-center distances (d\*) between the aggregate layers can be calculated from the peak positions ( $d^* = 2\pi/q^*$ , as detailed in the Supporting Information) and are 29 Å (C<sub>26</sub>PA<sub>2</sub>) and 55 Å (C<sub>48</sub>PA<sub>2</sub>) at 30 °C. A higher value in C<sub>48</sub>PA<sub>2</sub> for d\* compared to the short chain analogue is expected because the interlayer spacing strongly depends on the polymer length. The layer spacings remain relatively constant throughout the complete cooling process ( $\pm 2$  Å). The domain sizes along the layer normal can be calculated with the Scherrer equation ( $\xi_L = 2\pi/\Delta q$ ,  $\Delta q$  being the full width at half-maximum of q\*). For C<sub>26</sub>PA<sub>2</sub>, the domain size is 900 Å when the backbone is melted and decreases to 500 Å when the backbone is crystalline. For C<sub>48</sub>PA<sub>2</sub>, the domain size along the layer normal is as large as 2800 Å when the backbone is melted, but we note that the layers coexist with some acid groups in the disordered state. The domain size then similarly decreases to 500 Å upon the crystallization of the PE backbone. This much higher extent of order in the layered aggregates when the PE backbone is amorphous is likely a result of the greater polymer backbone mobility, that produces better uniformity across the samples. We also note that the domain sizes of ~500 Å at room temperature are significantly larger than the domain sizes of 170 and 350 Å in the carboxylate telechelic analogues,  $C_{21}(COOH)_2$  and  $C_{46}(COOH)_2$ , respectively. Tilt angle  $\theta$  between the polyethylene chains and the layer normal are calculated from d\* and the length of the all-trans chain conformation added to the approximate length of the head groups (for definition of the tilt angle, see Figure S2). <sup>41</sup> This yields tilt angles of 45°  $(C_{26}PA_2)$  and 36°  $(C_{48}PA_2)$ , assuming chain lengths of 40.8 and 68.5 Å, respectively. A larger tilt for the shorter  $C_{26}PA_2$  is attributed to a greater amount of steric hindrance in the system resulting from the higher volume fraction of head groups. These tilt angles are comparable to the carboxylate analogues  $C_{21}(COOH)_2$  and  $C_{46}(COOH)_2$ , which tilt at 42° and 35°, respectively. <sup>17</sup>

As previously described, the PE segments of  $C_{26}\text{PA}_2$  and  $C_{48}\text{PA}_2$  are amorphous and exist with layered acid aggregates between  $T_{\rm m}$  and  $T_{\rm dis}$ , above which the layered aggregates break apart. A similar phenomenon has been reported in phosphonic acid functionalized materials by Liang et al. wherein the layered morphology was described as a thermotropic liquid crystalline (LC) phase. To explore this phase behavior further,  $C_{26}\text{PA}_2$  was investigated by PLM in the isotropic melt above  $T_{\rm dis.}$  and in the liquid crystalline state between  $T_{\rm dis.}$  and  $T_{\rm m}$ . Under crossed polarizers, the smectic liquid crystalline phase displays characteristic cross-like interference patterns consistent with periodic layers emanating from a central position (Figure 5). The smechanism of the polymers of the polymers of the property of the propert

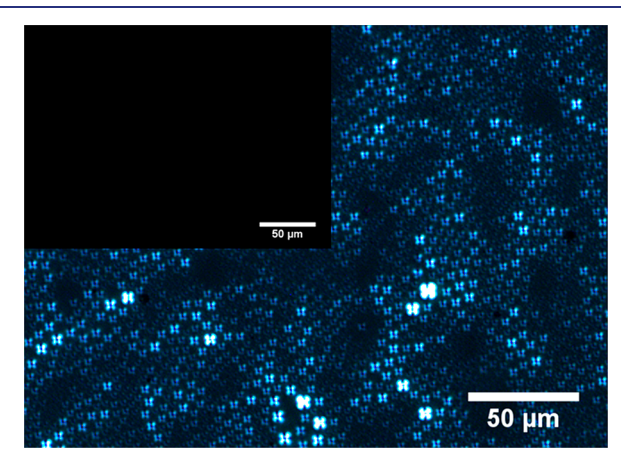
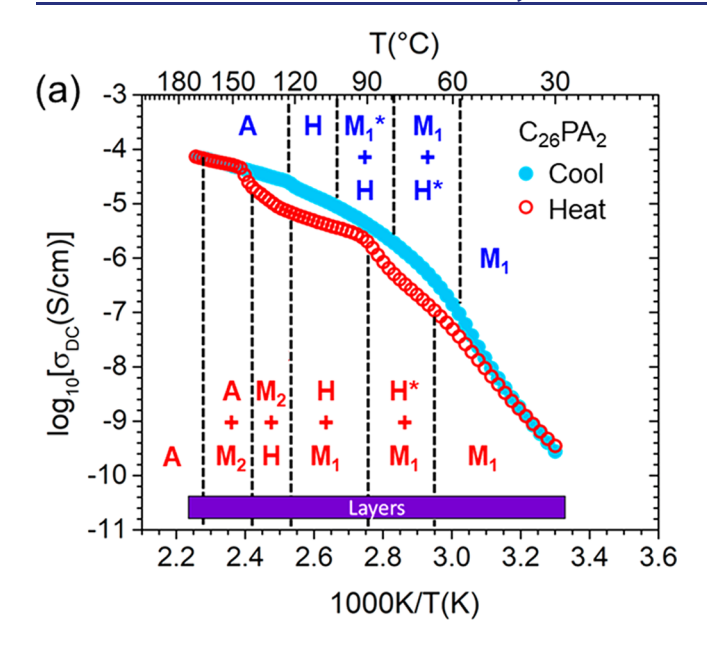
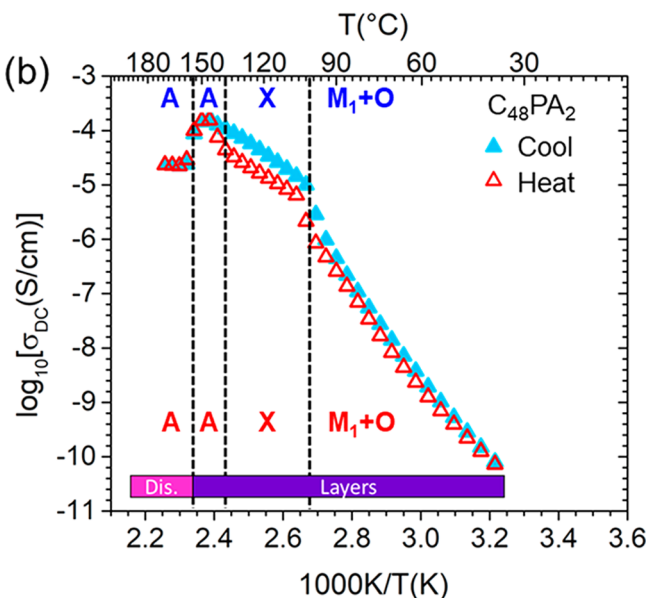


Figure 5. PLM images with crossed polarizers of  $C_{26}PA_2$ . (inset) The isotropic melt at 240 °C; (main image) liquid crystalline phase after cooling from 240 to 233 °C at 10 K/min and holding for 20 min (scale bar: 100  $\mu$ m). The diameters of these cross-like interference patterns are ~3  $\mu$ m.

the contrast originates from the alternating layers of crystalline and amorphous phases; in this liquid crystalline phase, the contrast arises from the index of refraction differences between the phosphonate and hydrocarbon portions of the telechelic polymers. Interestingly, upon being cooled below  $T_{\rm m}$ , the cross-like interference patterns in  $C_{26}PA_2$  persist indicating that as the PE backbone crystallizes, there is little rearrangement of the layered morphology, which is consistent with the X-ray scattering. The presence of LC phases has been reported previously for different phosphonic acid functionalized materials. The case of  $C_{26}PA_2$  and  $C_{48}PA_2$ , the LC phases are stable; this is consistent with the high strength of the hydrogen bonded network in these polymers and could be advantageous in various applications involving electroactive polymers, e.g., ionic polymeric transducers.

**Transport Properties.** The ionic conductivities of  $C_{26}PA_2$  and  $C_{48}PA_2$  were determined from 30 to 170 °C under dry conditions using electrochemical impedance spectroscopy (EIS) measurements (Figure 6). The bulk morphologies are also indicated. Previously, the telechelic carboxylate salts





**Figure 6.** Temperature dependence of ionic conductivity obtained from EIS measurements under dry conditions upon cooling (blue) and heating (red) in (a)  $C_{26}PA_2$  and (b)  $C_{48}PA_2$ . The packing of the PE segments as identified from X-ray scattering measurements are labeled and the transition temperatures represented by vertical dashed lines: A: amorphous, X: unknown phase, M1 and M2: two monoclinic phases, O: Orthorhombic phase, H: hexagonal phase. Phases marked with \* are the minority phase. The colored bars indicate phosphonate aggregate morphologies, which are either disordered (Dis.) or layered aggregates.

demonstrated Arrhenius-like behavior ( $\sigma_{DC} = \sigma_0 e^{-E_a/(RT)}$ , with  $\sigma_0$  defined as the conductivity at indefinitely high temperature and  $E_a$  as the activation energy for the ion conduction). This behavior originates from the decoupling of the ion movement from the polymer backbone segmental dynamics. Upon cooling, the conductivity of  $C_{26}PA_2$  in the liquid crystalline phase shows Arrhenius-like behavior above ~120 °C, the crystallization temperature of the PE backbone. While this occurs when the backbone is melted and there may be some chain mobility, this linear relationship suggests that proton

motion is dominated by the dynamics within the phosphonate, rather than the segmental dynamics. The non-Arrhenius behavior of the conductivity below the melting/crystallizing indicates the role of segmental dynamics and other structural changes in the bulk. The hysteresis in the structural changes and the conductivity upon cooling and heating in  $C_{26}PA_2$  are reproducible and thus are not attributable to material decomposition. Note that  $C_{48}PA_2$  exhibits an abrupt increase in conductivity at ~155 °C, which corresponds to the transition upon cooling from disordered aggregates to a liquid crystalline structure of layered aggregates and amorphous PE backbones (see Figure 7). This change in conductivity is

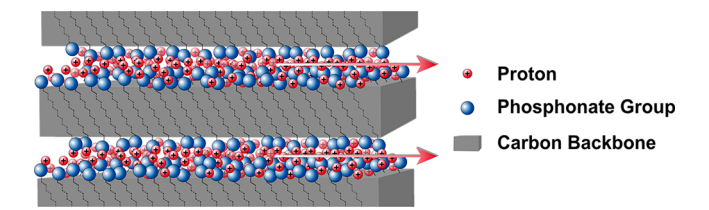


**Figure 7.** Schematic representation of proton transport within the layered aggregates. Dashed lines are representative for  $\rm C_{26^-}$  and  $\rm C_{48^-}$  segments.

reversible and comparable in magnitude upon heating and cooling, and highlights the advantage of self-assembled phosphonic acid aggregates (as compared to disordered morphologies) with respect to transport properties, which is consistent with Steininger et al. <sup>14</sup> In the case of  $C_{26}PA_2$ , the layered aggregate morphology is present at all temperatures tested with EIS, and thus a significant jump in conductivity could not be observed between the disordered and liquid crystalline morphologies.

In the thermotropic LC regime, when the aggregates are layered and the backbone is melted, both C<sub>26</sub>PA<sub>2</sub> and C<sub>48</sub>PA<sub>2</sub> exhibit proton conductivities of  $\sim 10^{-4}$  S/cm, specifically 5.1  $\times$  $10^{-5}$  S/cm and 1.5 ×  $10^{-4}$  S/cm at 150 °C, respectively. C<sub>48</sub>PA<sub>2</sub> unexpectedly has a higher conductivity than C<sub>26</sub>PA<sub>2</sub> in this LC regime, even though C48PA2 has a lower charge concentration. The ion-exchange capacity, IEC, of C<sub>48</sub>PA<sub>2</sub> is 4.8 mmol/g, compared to an IEC of 7.0 mmol/g in C<sub>26</sub>PA<sub>2</sub>. A possible reason for this faster proton transport is a more advantageous hierarchical structure for ion conduction in C<sub>48</sub>PA<sub>2</sub>. The domain size of 2800 Å in C<sub>48</sub>PA<sub>2</sub>, as previously discussed, may lead to more uniformity and longer pathways for the protons to travel as compared to the domain size of 500 Å in C<sub>26</sub>PA<sub>2</sub>. Previous studies of proton conducting polymers aligned by mechanical shearing demonstrated that the improved long-range order increased the anhydrous proton conductivity in the LC state. 51-53 We note that while the maximum conductivity reached in the LC regime by C<sub>48</sub>PA<sub>2</sub> is  $1.5 \times 10^{-4}$  S/cm at 150 °C, the conductivity of C<sub>26</sub>PA<sub>2</sub> reaches  $7.3 \times 10^{-5}$  S/cm at 180 °C, the maximum temperature measured, and may continue to increase with temperature until  $T_{\rm dis}$  at ~234 °C.

Considering the absence of both water and additives in the phosphonic acid functionalized materials reported here, the conductivity is high and on par with or exceeds that of other recently studied phosphonic acid functionalized polymers. Atanasov et al. reported a poly(2,3,5,6-tetrafluorostyrene-4-phosphonic acid), PWN70 (IEC = 6.6 mmol/g), with anhydrous proton conductivity of  $7.3 \times 10^{-6}$  S/cm at

150 °C, significantly lower than both C<sub>26</sub>PA<sub>2</sub> and C<sub>48</sub>PA<sub>2</sub> at that temperature. 46 However, we note that the conductivity of PWN70 reaches  $1.6 \times 10^{-4}$  S/cm at 220 °C, the maximum temperature measured. The phosphonic acid functionalized materials presented by Liang et al. exhibit thermotropic LC phases, and the system with the highest concentration (IEC = 3.5 mmol/g) shows the highest proton conductivity, 5.5  $\times$  $10^{-5}$  S/cm at 150 °C, <sup>33</sup> and increases further to 2.3 ×  $10^{-4}$  S/ cm at 200 °C in the LC regime. Therefore, in addition to charge concentration, both the mobility of the polymer backbone and the nanoscale structure of the ionic aggregates impact proton transport, and these attributes merit further investigation in future work. To further increase the transport abilities of these materials, a macroscopic alignment of the materials in the LC phase could be advantageous to decrease the presence of grain boundaries. The promising conductivities of C<sub>26</sub>PA<sub>2</sub> and C<sub>48</sub>PA<sub>2</sub> compared to other phosphonated polymers in addition to the pronounced ordering of the phosphonic acid aggregates presents opportunities to further develop these telechelic polymers. For example, intermediate length between 26 and 48 carbons will increase charge concentration over C<sub>48</sub>PA<sub>2</sub>, while having improved long-range order relative to C<sub>26</sub>PA<sub>2</sub>. Moreover, precise positioning of functional groups is likely key to designing self-assembled and liquid crystalline morphologies for highly conductive, advanced proton exchange membranes.

# CONCLUSION

Phosphonic acid-terminated polyethylene telechelics with precise chain lengths can be accessed by straightforward synthetic protocols. Simple reaction conditions with readily available substrates were implemented that yield quantitative conversions of the starting materials and are applicable to increased batch sizes, which makes this approach valuable for industrial applications. The thermal properties suggest these materials are suitable as proton conductors at intermediate operating temperatures (~150 °C) in fuel cells without undesired condensation reactions occurring. Layered aggregates of the phosphonic acid groups prevail below and above the melting transition of the PE backbones and transition to a disordered state at  $\sim$ 80 °C above  $T_{\rm m}$  for  $C_{26}PA_2$  and  $\sim$ 20 °C for C<sub>48</sub>PA<sub>2</sub>. At 150 °C, when the backbone is melted, the proton conductivities through the layered aggregates in C<sub>26</sub>PA<sub>2</sub> and  $C_{48}PA_2$  reach 5.1 × 10<sup>-5</sup> S/cm and 1.5 × 10<sup>-4</sup> S/cm, respectively, though the maximum conductivity of C<sub>26</sub>PA<sub>2</sub> may be higher at yet-unexplored temperatures greater than 180 °C. The beneficial impact of the layered aggregate morphology on the proton conductivity is evident in C<sub>48</sub>PA<sub>2</sub> by the significant loss in conductivity at higher temperatures corresponding to a disordered state. The wide temperature ranges of these liquid crystalline states make these materials interesting for use as electro-active polymers in high-performance actuators and sensors. These applications merit further exploration. Additionally, alignment strategies via mechanical shearing or templating could be applied to these telechelic polymers to further increase their proton conductivity. The presented systematic approach toward the understanding of proton transport in structured phosphonic acid functionalized materials suggests that the development of next-generation proton exchange membranes will benefit from highly ordered self-assembled nanoscale morphologies.

## ASSOCIATED CONTENT

# Supporting Information

General remarks; Experimental methods; Thermal stability test with  $^{31}P$  NMR spectroscopy; additional X-ray scattering data during heating and cooling and positions of identified peaks; analysis of domain sizes ( $\xi$ ) vs. temperature; NMR spectra of all compounds and intermediates. The Supporting Information is available free of charge at https://pubs.acs.org/doi/10.1021/jacs.1c08031.

(PDF)

#### AUTHOR INFORMATION

# **Corresponding Authors**

Stefan Mecking – Department of Chemistry, University of Konstanz, 78457 Konstanz, Germany; orcid.org/0000-0002-6618-6659; Email: stefan.mecking@uni.kn

Karen I. Winey — Department of Materials Science and Engineering, University of Pennsylvania, Philadelphia, Pennsylvania 19104, United States; oorcid.org/0000-0001-5856-3410; Email: winey@seas.upenn.edu

#### **Authors**

Anne Staiger – Department of Chemistry, University of Konstanz, 78457 Konstanz, Germany; orcid.org/0000-0002-6103-4402

Benjamin A. Paren — Department of Materials Science and Engineering, University of Pennsylvania, Philadelphia, Pennsylvania 19104, United States; orcid.org/0000-0002-4361-5182

Robin Zunker – Department of Chemistry, University of Konstanz, 78457 Konstanz, Germany

Son Hoang — Department of Materials Science and Engineering, University of Pennsylvania, Philadelphia, Pennsylvania 19104, United States

Manuel Häußler – Department of Chemistry, University of Konstanz, 78457 Konstanz, Germany

Complete contact information is available at: https://pubs.acs.org/10.1021/jacs.1c08031

## **Author Contributions**

§A.S. and B.A.P. contributed equally to this work.

#### Notes

The authors declare no competing financial interest.

# ACKNOWLEDGMENTS

Funding by the Baden-Württemberg Foundation (project "PRICON") is gratefully acknowledged. We thank Marina Krumova for Polarized Light Microscopy measurements, and Adrian Donner and Doreen Herzog for ESI-HRMS measurements. K.I.W. and B.A.P. acknowledge funding from the National Science Foundation (NSF) DMR 1904767 and NSF PIRE 1545884. We also acknowledge the use of the Dual Source and Environmental X-ray Scattering facility operated by the Laboratory for Research on the Structure of Matter at the University of Pennsylvania (NSF MRSEC 17- 20530). The equipment purchase was made possible by a NSF MRI grant (17-25969), an ARO DURIP grant (W911NF-17- 1-0282), and the University of Pennsylvania.

# REFERENCES

(1) Mauritz, K. A.; Moore, R. B. State of Understanding of Nafion. *Chem. Rev.* **2004**, *104* (10), 4535–4586.

- (2) Kusoglu, A.; Weber, A. Z. New Insights into Perfluorinated Sulfonic-Acid Ionomers. *Chem. Rev.* **2017**, *117* (3), 987–1104.
- (3) Peighambardoust, S. J.; Rowshanzamir, S.; Amjadi, M. Review of the proton exchange membranes for fuel cell applications. *Int. J. Hydrogen Energy* **2010**, 35 (17), 9349–9384.
- (4) Zawodzinski, T. A. Water Uptake by and Transport Through Nafion® 117 Membranes. *J. Electrochem. Soc.* **1993**, *140* (4), 1041.
- (5) Alberti, G.; Casciola, M.; Massinelli, L.; Bauer, B. Polymeric proton conducting membranes for medium temperature fuel cells (110–160°C). *J. Membr. Sci.* **2001**, *185* (1), 73–81.
- (6) Chandan, A.; Hattenberger, M.; El-Kharouf, A.; Du, S.; Dhir, A.; Self, V.; Pollet, B. G.; Ingram, A.; Bujalski, W. High temperature (HT) polymer electrolyte membrane fuel cells (PEMFC) A review. *J. Power Sources* **2013**, 231, 264–278.
- (7) Rosli, R. E.; Sulong, A. B.; Daud, W. R. W.; Zulkifley, M. A.; Husaini, T.; Rosli, M. I.; Majlan, E. H.; Haque, M. A. A review of high-temperature proton exchange membrane fuel cell (HT-PEMFC) system. *Int. J. Hydrogen Energy* **2017**, 42 (14), 9293–9314.
- (8) Araya, S. S.; Zhou, F.; Liso, V.; Sahlin, S. L.; Vang, J. R.; Thomas, S.; Gao, X.; Jeppesen, C.; Kær, S. K. A comprehensive review of PBI-based high temperature PEM fuel cells. *Int. J. Hydrogen Energy* **2016**, 41 (46), 21310–21344.
- (9) Miyatake, K.; Hay, A. S. New poly(arylene ether)s with pendant phosphonic acid groups. *J. Polym. Sci., Part A: Polym. Chem.* **2001**, 39 (21), 3770–3779.
- (10) Schuster, M.; Kreuer, K.-D.; Steininger, H.; Maier, J. Proton conductivity and diffusion study of molten phosphonic acid H3PO3. *Solid State Ionics* **2008**, *179* (15), 523–528.
- (11) Jung, H. Y.; Kim, S. Y.; Kim, O.; Park, M. J. Effect of the Protogenic Group on the Phase Behavior and Ion Transport Properties of Acid-Bearing Block Copolymers. *Macromolecules* **2015**, 48 (17), 6142–6152.
- (12) Paddison, S. J.; Kreuer, K.-D.; Maier, J. About the choice of the protogenic group in polymer electrolyte membranes: Ab initio modelling of sulfonic acid, phosphonic acid, and imidazole functionalized alkanes. *Phys. Chem. Chem. Phys.* **2006**, 8 (39), 4530–4542.
- (13) Meng, Y. Z.; Tjong, S. C.; Hay, A. S.; Wang, S. J. Proton-exchange membrane electrolytes derived from phosphonic acid containing poly(arylene ether)s. *Eur. Polym. J.* **2003**, 39 (3), 627–631.
- (14) Steininger, H.; Schuster, M.; Kreuer, K. D.; Kaltbeitzel, A.; Bingöl, B.; Meyer, W. H.; Schauff, S.; Brunklaus, G.; Maier, J.; Spiess, H. W. Intermediate temperature proton conductors for PEM fuel cells based on phosphonic acid as protogenic group: A progress report. *Phys. Chem. Chem. Phys.* **2007**, *9* (15), 1764–1773.
- (15) Jang, S.; Kim, S. Y.; Jung, H. Y.; Park, M. J. Phosphonated Polymers with Fine-Tuned Ion Clustering Behavior: Toward Efficient Proton Conductors. *Macromolecules* **2018**, *51* (3), 1120–1128.
- (16) Rank, C.; Yan, L.; Mecking, S.; Winey, K. I. Periodic Polyethylene Sulfonates from Polyesterification: Bulk and Nanoparticle Morphologies and Ionic Conductivities. *Macromolecules* **2019**, 52 (21), 8466–8475.
- (17) Yan, L.; Häußler, M.; Bauer, J.; Mecking, S.; Winey, K. I. Monodisperse and Telechelic Polyethylenes Form Extended Chain Crystals with Ionic Layers. *Macromolecules* **2019**, 52 (13), 4949–4956.
- (18) Yan, L.; Rank, C.; Mecking, S.; Winey, K. I. Gyroid and Other Ordered Morphologies in Single-Ion Conducting Polymers and Their Impact on Ion Conductivity. *J. Am. Chem. Soc.* **2020**, *142* (2), 857–866
- (19) Trigg, E. B.; Stevens, M. J.; Winey, K. I. Chain Folding Produces a Multilayered Morphology in a Precise Polymer: Simulations and Experiments. *J. Am. Chem. Soc.* **2017**, *139* (10), 3747–3755.
- (20) Frischknecht, A. L.; Paren, B. A.; Middleton, L. R.; Koski, J. P.; Tarver, J. D.; Tyagi, M.; Soles, C. L.; Winey, K. I. Chain and Ion Dynamics in Precise Polyethylene Ionomers. *Macromolecules* **2019**, *52* (20), 7939–7950.
- (21) Paren, B. A.; Thurston, B. A.; Neary, W. J.; Kendrick, A.; Kennemur, J. G.; Stevens, M. J.; Frischknecht, A. L.; Winey, K. I.

- Percolated Ionic Aggregate Morphologies and Decoupled Ion Transport in Precise Sulfonated Polymers Synthesized by Ring-Opening Metathesis Polymerization. *Macromolecules* **2020**, 53 (20), 8960–8973.
- (22) Paren, B. A.; Thurston, B. A.; Kanthawar, A.; Neary, W. J.; Kendrick, A.; Maréchal, M.; Kennemur, J. G.; Stevens, M. J.; Frischknecht, A. L.; Winey, K. I. Fluorine-Free Precise Polymer Electrolyte for Efficient Proton Transport: Experiments and Simulations. *Chem. Mater.* **2021**, 33 (15), 6041–6051.
- (23) Trigg, E. B.; Gaines, T. W.; Maréchal, M.; Moed, D. E.; Rannou, P.; Wagener, K. B.; Stevens, M. J.; Winey, K. I. Self-assembled highly ordered acid layers in precisely sulfonated polyethylene produce efficient proton transport. *Nat. Mater.* **2018**, 17 (8), 725–731.
- (24) Atanasov, V.; Oleynikov, A.; Xia, J.; Lyonnard, S.; Kerres, J. Phosphonic acid functionalized poly(pentafluorostyrene) as polyelectrolyte membrane for fuel cell application. *J. Power Sources* **2017**, 343, 364–372.
- (25) Parvole, J.; Jannasch, P. Polysulfones Grafted with Poly-(vinylphosphonic acid) for Highly Proton Conducting Fuel Cell Membranes in the Hydrated and Nominally Dry State. *Macromolecules* **2008**, *41* (11), 3893–3903.
- (26) Subianto, S.; Choudhury, N. R.; Dutta, N. K. Palladium-catalyzed phosphonation of SEBS block copolymer. *J. Polym. Sci., Part A: Polym. Chem.* **2008**, 46 (16), 5431–5441.
- (27) Opper, K. L.; Markova, D.; Klapper, M.; Müllen, K.; Wagener, K. B. Precision Phosphonic Acid Functionalized Polyolefin Architectures. *Macromolecules* **2010**, *43* (8), 3690–3698.
- (28) Buitrago, C. F.; Alam, T. M.; Opper, K. L.; Aitken, B. S.; Wagener, K. B.; Winey, K. I. Morphological Trends in Precise Acidand Ion-Containing Polyethylenes at Elevated Temperature. *Macromolecules* **2013**, *46* (22), 8995–9002.
- (29) Buitrago, C. F.; Jenkins, J. E.; Opper, K. L.; Aitken, B. S.; Wagener, K. B.; Alam, T. M.; Winey, K. I. Room Temperature Morphologies of Precise Acid- and Ion-Containing Polyethylenes. *Macromolecules* **2013**, 46 (22), 9003–9012.
- (30) Martínez-Felipe, A. Liquid crystal polymers and ionomers for membrane applications. *Liq. Cryst.* **2011**, 38 (11–12), 1607–1626.
- (31) Kato, T.; Mizoshita, N.; Kishimoto, K. Functional Liquid-Crystalline Assemblies: Self-Organized Soft Materials. *Angew. Chem., Int. Ed.* **2006**, 45 (1), 38–68.
- (32) Kato, T.; Yoshio, M.; Ichikawa, T.; Soberats, B.; Ohno, H.; Funahashi, M. Transport of ions and electrons in nanostructured liquid crystals. *Nature Reviews Materials* **2017**, 2 (4), 17001.
- (33) Liang, T.; Tan, S.; Cao, S.; Wu, Y. Synthesis and characterization of proton conductive liquid crystals bearing phosphonic acid moieties. *J. Mol. Struct.* **2017**, *1150*, 574–579.
- (34) Noonan, K. J. T.; Hugar, K. M.; Kostalik, H. A.; Lobkovsky, E. B.; Abruña, H. D.; Coates, G. W. Phosphonium-Functionalized Polyethylene: A New Class of Base-Stable Alkaline Anion Exchange Membranes. *J. Am. Chem. Soc.* **2012**, *134* (44), 18161–18164.
- (35) Buggy, N. C.; Du, Y.; Kuo, M.-C.; Ahrens, K. A.; Wilkinson, J. S.; Seifert, S.; Coughlin, E. B.; Herring, A. M. A Polyethylene-Based Triblock Copolymer Anion Exchange Membrane with High Conductivity and Practical Mechanical Properties. *ACS Applied Polymer Materials* **2020**, 2 (3), 1294–1303.
- (36) Zhu, L.; Yu, X.; Peng, X.; Zimudzi, T. J.; Saikia, N.; Kwasny, M. T.; Song, S.; Kushner, D. I.; Fu, Z.; Tew, G. N.; Mustain, W. E.; Yandrasits, M. A.; Hickner, M. A. Poly(olefin)-Based Anion Exchange Membranes Prepared Using Ziegler-Natta Polymerization. *Macromolecules* **2019**, *52* (11), 4030–4041.
- (37) Khurana, R.; Schaefer, J. L.; Archer, L. A.; Coates, G. W. Suppression of Lithium Dendrite Growth Using Cross-Linked Polyethylene/Poly(ethylene oxide) Electrolytes: A New Approach for Practical Lithium-Metal Polymer Batteries. J. Am. Chem. Soc. 2014, 136 (20), 7395–7402.
- (38) Jian, Z.; Falivene, L.; Boffa, G.; Sánchez, S. O.; Caporaso, L.; Grassi, A.; Mecking, S. Direct Synthesis of Telechelic Polyethylene by

- Selective Insertion Polymerization. Angew. Chem., Int. Ed. 2016, 55 (46), 14378–14383.
- (39) Nzahou Ottou, W.; Norsic, S.; Belaid, I.; Boisson, C.; D'Agosto, F. Amino End-Functionalized Polyethylenes and Corresponding Telechelics by Coordinative Chain Transfer Polymerization. *Macromolecules* **2017**, 50 (21), 8372–8377.
- (40) Norsic, S.; Thomas, C.; D'Agosto, F.; Boisson, C. Divinyl-End-Functionalized Polyethylenes: Ready Access to a Range of Telechelic Polyethylenes through Thiol-Ene Reactions. *Angew. Chem., Int. Ed.* **2015**, *54* (15), 4631–4635.
- (41) Rank, C.; Häußler, M.; Rathenow, P.; King, M.; Globisch, C.; Peter, C.; Mecking, S. Anisotropic Extended-Chain Polymer Nanocrystals. *Macromolecules* **2019**, *52* (16), 6142–6148.
- (42) Witt, T.; Häußler, M.; Kulpa, S.; Mecking, S. Chain Multiplication of Fatty Acids to Precise Telechelic Polyethylene. *Angew. Chem., Int. Ed.* **2017**, *56* (26), 7589–7594.
- (43) Ngo, H. L.; Jones, K.; Foglia, T. A. Metathesis of unsaturated fatty acids: Synthesis of long-chain unsaturated- $\alpha$ , $\omega$ -dicarboxylic acids. *J. Am. Oil Chem. Soc.* **2006**, 83 (7), 629–634.
- (44) Fiedler, T.; Barbasiewicz, M.; Stollenz, M.; Gladysz, J. A. Nonmetal-templated approaches to bis(borane) derivatives of macrocyclic dibridgehead diphosphines via alkene metathesis. *Beilstein J. Org. Chem.* **2018**, *14*, 2354–2365.
- (45) McKenna, C. E.; Higa, M. T.; Cheung, N. H.; McKenna, M.-C. The facile dealkylation of phosphonic acid dialkyl esters by bromotrimethylsilane. *Tetrahedron Lett.* **1977**, *18* (2), 155–158.
- (46) Atanasov, V.; Lee, A. S.; Park, E. J.; Maurya, S.; Baca, E. D.; Fujimoto, C.; Hibbs, M.; Matanovic, I.; Kerres, J.; Kim, Y. S. Synergistically integrated phosphonated poly(pentafluorostyrene) for fuel cells. *Nat. Mater.* **2021**, *20*, 370–377.
- (47) Schuster, M.; Rager, T.; Noda, A.; Kreuer, K. D.; Maier, J. About the Choice of the Protogenic Group in PEM Separator Materials for Intermediate Temperature, Low Humidity Operation: A Critical Comparison of Sulfonic Acid, Phosphonic Acid and Imidazole Functionalized Model Compounds. Fuel Cells 2005, 5 (3), 355–365.
- (48) Russell, K. E.; Hunter, B. K.; Heyding, R. D. Monoclinic polyethylene revisited. *Polymer* 1997, 38 (6), 1409–1414.
- (49) Dierking, I., in *Textures of liquid crystals*; John Wiley & Sons, 2003; p 33-41.
- (50) Kumar, K. R. S.; Gupta, M.; Sakamoto, T.; Kato, T. Thermotropic Columnar Liquid Crystals Based on Wedge-Shaped Phenylphosphonic Acids. *Bull. Chem. Soc. Jpn.* **2019**, 92 (9), 1450–1452.
- (51) Tan, S.; Wang, C.; Wu, Y. Anisotropic assembly of a side chain liquid crystal polymer containing sulfoalkoxy groups for anhydrous proton conduction. *J. Mater. Chem. A* **2013**, *1* (4), 1022–1025.
- (52) Yang, X.; Tan, S.; Liang, T.; Wei, B.; Wu, Y. A unidomain membrane prepared from liquid-crystalline poly(pyridinium 4-styrene sulfonate) for anhydrous proton conduction. *J. Membr. Sci.* **2017**, *523*, 355–360.
- (53) Ueda, S.; Kagimoto, J.; Ichikawa, T.; Kato, T.; Ohno, H. Anisotropic Proton-Conductive Materials Formed by the Self-Organization of Phosphonium-Type Zwitterions. *Adv. Mater.* **2011**, 23 (27), 3071–3074.